

# Journal of Materials Chemistry A

Accepted Manuscript

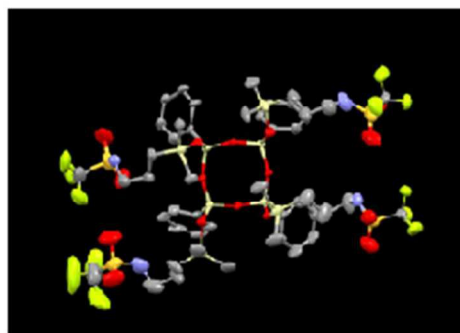
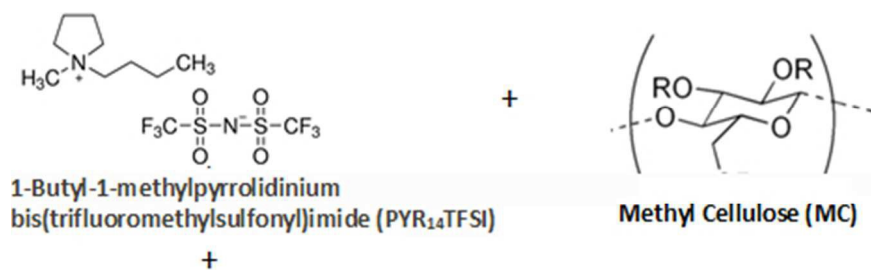
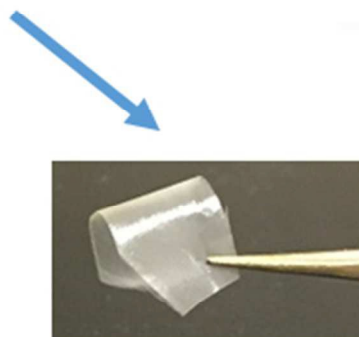


This is an *Accepted Manuscript*, which has been through the Royal Society of Chemistry peer review process and has been accepted for publication.

*Accepted Manuscripts* are published online shortly after acceptance, before technical editing, formatting and proof reading. Using this free service, authors can make their results available to the community, in citable form, before we publish the edited article. We will replace this *Accepted Manuscript* with the edited and formatted *Advance Article* as soon as it is available.

You can find more information about *Accepted Manuscripts* in the [Information for Authors](#).

Please note that technical editing may introduce minor changes to the text and/or graphics, which may alter content. The journal's standard [Terms & Conditions](#) and the [Ethical guidelines](#) still apply. In no event shall the Royal Society of Chemistry be held responsible for any errors or omissions in this *Accepted Manuscript* or any consequences arising from the use of any information it contains.

4 mer - (LiTFSI)<sub>4</sub>

$$t_{\text{Li}^+} = 0.37$$

$$\text{Conductivity } (\sigma) = 3 \times 10^{-4} \text{ S/cm}$$

**“Multi-ionic lithium salts increase lithium ion transference numbers in ionic liquid gel separators”**

Parameswara Rao Chinnam<sup>1</sup>, Vijay Chatare<sup>1</sup>, Sumanth Chereddy<sup>1</sup>, Ramya Mantravadi<sup>1</sup>, Michael Gau<sup>1</sup>,  
Joe Schwab<sup>2</sup> and Stephanie L. Wunder\*

<sup>1</sup>Department of Chemistry, Temple University, Philadelphia, PA 19122

<sup>2</sup>Hybrid Plastics, Hattiesburg, MS 39401

**Abstract**

Solid ion-gel separators for lithium or lithium ion batteries have been prepared with high lithium ion transference numbers ( $t_{Li^+} = 0.36$ ), high room temperature ionic conductivities ( $\sigma \rightarrow 10^{-3}$  S/cm), and moduli in the MPa range. These were formed from the room temperature ionic liquid 1-butyl-1-methylpyrrolidinium bis(trifluoromethylsulfonyl)imide (PYR<sub>14</sub>TFSI), a polysilsesquioxane multi-ionic lithium salt that contains four phenyl groups and four pendent LiTFSI (4mer-(LiTFSI)<sub>4</sub>) on a SiO<sub>1.5</sub> ring, and methyl cellulose (MC). After co-dissolution in dimethylsulfonamide (DMSO) and evaporation of the DMSO, ion-gels were formed at different PYR<sub>14</sub>TFSI/MC ratios but at constant 0.25 M 4mer-(LiTFSI)<sub>4</sub>. Conductivity decreased but  $t_{Li^+}$  increased with increased MC content. Differential scanning calorimetry, dynamical mechanical analysis and X-ray diffraction data indicated that the PYR<sub>14</sub>TFSI/MC/4mer-(LiTFSI)<sub>4</sub> ion gels were micro-phase separated into a conductive PYR<sub>14</sub>TFSI/4mer-(LiTFSI)<sub>4</sub> phase and one in which the MC was swollen with PYR<sub>14</sub>TFSI/4mer-(LiTFSI)<sub>4</sub>. The high  $t_{Li^+}$  was attributed to the large size of the anion, its decreased ability as the result of its rigid structure to form ion aggregates, hydrophobic/hydrogen bonding interactions of the 4mer-(TFSI)<sub>4</sub> anion with MC, and participation of the MC hydroxyl groups in the solvation sphere of Li<sup>+</sup>, weakening its interaction with the 4mer-(TFSI)<sub>4</sub> and TFSI anions. The high moduli were the result of the preserved semi-crystalline, high glass transition ( $T_g$ ), fibrillar structure of MC in the ion gels.

**Introduction**

Room temperature ionic liquids (RTILs) have recently been investigated for lithium and lithium ion battery (LIB) applications due to their nonvolatility and thus lack of (or much reduced) flammability and increased safety<sup>2-5</sup>. RTILs can have ionic conductivities of  $10^{-2}$  S/cm<sup>6</sup>. Since in LIBs the only electroactive species is the Li<sup>+</sup> ion, which is transported between the anode and the cathode, a lithium salt, LiX (X<sup>-</sup> = anion), at 0.25- 1.2 M concentrations is added to the RTIL to form the electrolyte. Both LiX and the RTIL typically have the same anion, since the amount of dissolvable lithium is higher than in mixtures with dissimilar anions<sup>2</sup>. Disadvantages of RTILs and RTIL/LiXs include higher viscosities<sup>7-9</sup> and thus lower ionic conductivities<sup>10</sup> compared with commonly used aprotic electrolytes, with conductivity decreasing as the LiX concentration increases in the RTIL<sup>7-9</sup>. Further, RTIL/LiXs have low lithium ion transference numbers ( $t_{Li^+}$ ), the fraction of the charge carried by the electroactive Li<sup>+</sup> ions. In LIBs, high values of  $t_{Li^+}$  are desirable to increase the power density of LIBs, while low values result in polarization in the electrolyte, and this gradient in ionic concentration can cause large internal resistances. Slow Li<sup>+</sup> diffusion has been attributed to the strong coordination of the small Li<sup>+</sup> cation to the anions, resulting in [Li(X)<sub>n</sub>]<sup>(n-1)-</sup> aggregates<sup>11-15</sup>, with diffusion occurring not by a vehicular mechanism (where the Li<sup>+</sup> ion moves with the whole coordination shell, in clusters of [Li(TFSI)<sub>n</sub>]<sup>(n-1)-</sup>), but by a structure-diffusion mechanism (with disruption and formation of the coordination shells of Li<sup>+</sup> with TFSI anions<sup>15</sup>

<sup>17</sup>, and exchange of TFSI ligands believed to be only in the first coordination shell of  $\text{Li}^+$ <sup>11</sup>, so that the lithium ion transference number ( $t_{\text{Li}^+}$ ) is low. Diffusion coefficients, measured by pulse field gradient NMR, of ionic liquid anions, cations, and  $\text{Li}^+$  cations all decrease as the mole fraction ( $x$ ) of LiX increases, consistent with the conductivity decreases with increasing LiX<sup>10</sup>. Further, for LiX/RTIL mixtures, the diffusion coefficients decrease in the order  $D_{\text{cation}} > D_{\text{anion}} > D_{\text{Li}^+}$ <sup>7, 10, 15, 18, 19</sup>. There have been several approaches to increasing  $t_{\text{Li}^+}$  in LiX/RTIL pairs, in particular by (i) decreasing the diffusion coefficients of the anions or cations of the RTIL; (ii) Increasing the number density of  $\text{Li}^+$  ions; although increasing the mole fraction of LiX salt in the RTIL increases  $t_{\text{Li}^+}$  (to values of about 0.3)<sup>7, 10, 18-21</sup>, the concentration of the LiX salt in the RTILs is limited by their solubility and tendency of the mixtures to crystallize at high LiX concentrations<sup>19</sup>; (iii) addition of a third component, typically solvents with electronegative oxygens<sup>22-24</sup>, to RTIL/LiX solutions, in order to disrupt the coordination of  $\text{Li}^+$  and the anion of the RTIL, resulting in increased  $\text{Li}^+$  mobility and overall conductivity.

Nevertheless, the ionic conductivities of LiX/RTILs are still greater than those of solid polymer electrolytes (SPEs) ( $< 10^{-5}$  S/cm), and lithium ion transference numbers in polymers such as polyethylene oxide (PEO)/LiX are also low ( $t_{\text{Li}^+} \sim 0.2$ ). Further, compared with liquid electrolytes, SPEs have advantages such as processibility, ability to form thin, flexible films, and elimination of heavy containment materials that decrease gravimetric energy density. Therefore, when used in LIBs, it is preferable to incorporate the LiX/RTILs in the form of polymeric ion gels, with a view towards increasing the ionic conductivity of the polymer, maintaining sufficient mechanical strength to form flexible, thin membranes, but still retaining the safety advantages of SPEs when the liquid is a RTIL. Since a liquid is incorporated into the polymer, they are referred to as gel electrolytes, and when the liquid is a RTIL, they are often referred to as ion gels. The polymers in the RTIL/polymer/LiX systems that have been investigated include polyethylene oxide (PEO)<sup>25-28</sup>, and polyvinylidene fluoride (PVdF) or copolymers with hexafluoropropylene (PVdF-HFP)<sup>29, 30</sup>. Ion gels have also been prepared by solvent-free *in situ* polymerization of (3-aminopropyl)triethoxysilane (APTES) in PEO/RTIL/LiX<sup>31</sup>, by UV crosslinking<sup>32</sup>, and using functionalized silica nanoparticles<sup>33</sup>. Other methods include bicontinuous nanostructured polymer electrolyte membranes prepared by polymerization induced phase separation with components consisting of interpenetration and interpercolating bicontinuous domains of polyethylene oxide swollen with the RTIL/LiX, and highly cross-linked polystyrene<sup>34</sup>.

In this paper, we have synthesized a new multi-ionic lithium salt (**Figure 1**), all *cis*[( $\text{Ph}_4\text{Si}_4\text{O}_4(\text{OR})_4$ )]<sub>4</sub>, R =  $\text{Si}(\text{CH}_3)_2(\text{CH}_2)_3\text{NHSO}_2\text{CF}_3$ , referred to here as 4mer-(LiTFSI)<sub>4</sub>, and incorporated it into an ion gel composed of the RTIL 1-butyl-1-methylpyrrolidinium bis(trifluoromethylsulfonyl)imide (PYR<sub>14</sub>TFSI) and methyl cellulose (MC) as the gelator, with a view towards increasing  $t_{\text{Li}^+}$  and maintaining both high ionic conductivity and good mechanical properties in a solid electrolyte. These ion gels have been prepared using a method developed in our laboratory, in which gels are first formed using MC, *N,N*-dimethyl formamide (DMF) and a RTIL (PYR<sub>14</sub>TFSI). After removal of the DMF, solid ion gels remain that contain as little as 3 wt% MC, with the MC in the form of semicrystalline nano-fibrils that span the PYR<sub>14</sub>TFSI liquid, possible linked by MC chains that link two or more fibrils.<sup>1</sup>

Here ion gels were prepared using dimethylsulfoxide (DMSO) as the cosolvent, since the 4mer-(LiTFSI)<sub>4</sub> is not soluble in DMF. The PYR<sub>14</sub>TFSI was selected as the RTIL since: (i) it has a stability window of about 6V, sufficient for use in LIBs<sup>6</sup>; (ii) an imide anion,  $[\text{N}(\text{CF}_3\text{SO}_2)_2]^-$ , that is most effective at the

formation of a solid electrolyte interface (SEI) layer; (iii) inhibits dendrite growth on Li metal<sup>35</sup> and (iv) has the highest ionic conductivity when paired with the pyrrolidinium cation (PYR<sub>14</sub>)<sup>36</sup>, due to the highly electron-withdrawing nature of the trifluoromethyl substituents and delocalization of the negative charge<sup>37</sup>. The large mass of the silsesquioxane moiety (MW 4mer-(LiTFSI)<sub>4</sub> = 1564 g/mol), with four of these pendant anions, is expected to have reduced mobility compared with the single TFSI anion, thus decreasing its contribution to the conductivity, and increasing the contribution of the Li<sup>+</sup> cation. Further, hydrophobic as well as hydrogen bonding interactions between MC, 4mer-(LiTFSI)<sub>4</sub> and TFSI are expected to make more Li<sup>+</sup> cations available for conduction.

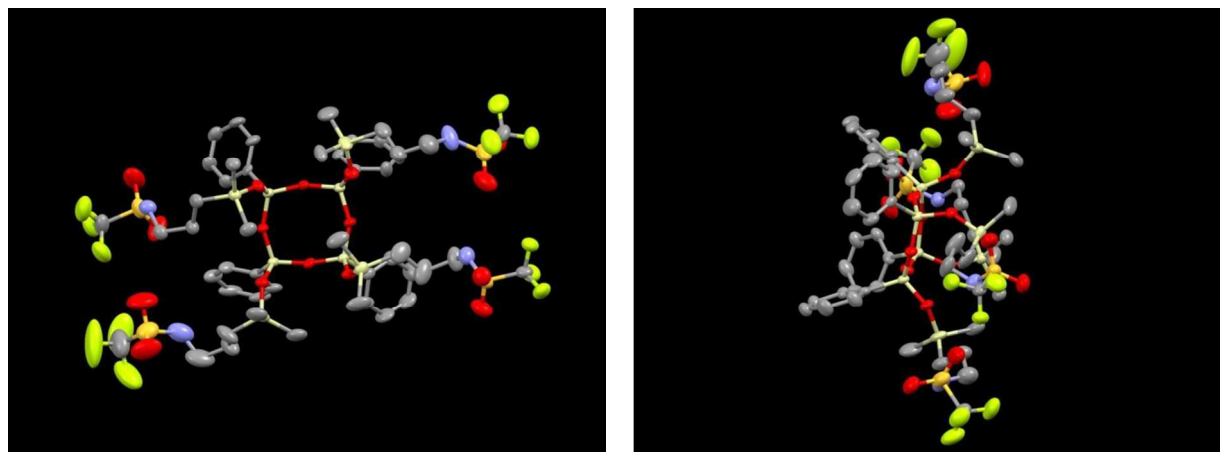


**Figure 1.** Two views of the single crystal structure of  $\text{Si}_8\text{S}_4\text{O}_{16}\text{N}_4\text{F}_{12}\text{C}_{48}\text{H}_{72} = \text{PhSi}_4\text{O}_4[(\text{Si}(\text{CH}_3)_2\text{-R})_4]$ , with  $\text{R} = \text{-CH}_2\text{CH}_2\text{CH}_2\text{NHSO}_2\text{CF}_3$ , presented as a thermal ellipsoid plot. Ellipsoids are shown at 30% probability. C atoms are shown as ball and stick models. C-H hydrogen atoms omitted for clarity.

● carbon; ● oxygen; ● fluorine; ● sulfur; ● nitrogen; ● silicon

## Experimental Section

### Materials

The 1-butyl-1-methylpyrrolidinium bis(trifluoromethylsulfonyl)imide ( $\text{C}_{11}\text{H}_{20}\text{F}_6\text{N}_2\text{O}_4\text{S}_2$ , MW 422.41, CAS Number 223437-11-4, was used as received (Alfa Aesar). This compound will be referred to here as PYR<sub>14</sub>TFSI. In the literature, 1-butyl-1-methylpyrrolidinium is also referred to as PYR<sub>14</sub>, P<sub>14</sub> (where subscripts describe number of carbons in each alkyl substituent<sup>38</sup>), [BuMePy]<sup>+</sup>, [BMP], and [bmpyr]; and bis(trifluoromethylsulfonyl)imide is referred to as TFSI, TFSA, and [NTf<sub>2</sub>]. Methyl cellulose (MC) (Sigma-Aldrich, primary supplier DOW, METHOCEL A), average molecular weight of 86,000, 27.5-31.5 wt% methoxy and a degree of substitution of 1.6-1.9 mol methoxy per mol cellulose (as specified by manufacturer) was dried at 70°C in vacuum before use. Bis(trifluoromethane)sulfonamide lithium salt (LiTFSI), anhydrous dimethyl sulfoxide (DMSO) and dimethyl formamide (DMF) were purchased from Sigma Aldrich and the DMSO and DMF further dried over molecular sieves before use. Lithium metal (0.75mm thick × 19mm wide) was purchased from Alfa-Aesar and stored in a desiccator inside an argon purged glove box.

## Characterization

**Differential scanning calorimetry (DSC)** was obtained on a TA Instruments Hi-Res DSC 2920 at 10 °C/min under N<sub>2</sub>. Except as noted, samples were scanned from 25 °C to 100 °C, 100 °C to -100 °C, and -100 °C to 100 °C, with the second heating scans reported. The glass transition temperature, T<sub>g</sub>, was taken as the midpoint of the heat capacity (C<sub>p</sub>) versus temperature plots. **Thermogravimetric analysis (TGA)** data was obtained on a TA Instruments 2950 (TA Instruments, New Castle, DE), scanned from 25 to 800 °C at a rate of 10 °C/min under N<sub>2</sub>. **Wide angle x-ray scattering (WAXS)** data was collected using a Bruker AXS D8 Discover X-ray diffractometer under N<sub>2</sub> purge. **Dynamic Mechanical Analysis (DMA)** of the blends was obtained with a TA Instruments DMA Q800 under N<sub>2</sub> purge. A pre-load force of 2.0 mN, a constant frequency of 1 Hz and a 15 μm amplitude were applied. Samples, ~ 12 mm length x 6.3 mm width x (0.01- 0.1mm) thickness, were equilibrated at -100 °C for 10 minutes. Measurements were taken from -100 °C to 250 °C with a heating rate of 2° C/min. **Electrochemical Measurements: Ionic conductivities** were measured by AC impedance spectroscopy using a Gamry potentiostat/galvanostat/ZRA (model interface 1000) in the frequency range from 0.01 to 1 MHz. Control of the equipment was through Gamry framework software and data was analyzed with Gamry Echem analysis software purchased from Gamry. Temperature dependent conductivities were obtained in a homemade electrochemical cell<sup>39</sup> (1 cm<sup>2</sup> stainless steel blocking electrodes) that was thermostatted in the oven of a cryogenic liquid N<sub>2</sub> gas chromatograph (GC). The electrochemical cell was placed in the oven of a GC and annealed overnight at 90°C. Conductivity measurements were made on the cooling cycle and heating cycles (the resistances on the heating and cooling cycles were very close) and the heating cycles are reported. At each temperature above RT, the sample was equilibrated for about 30 minutes. Conductivities, σ (mS/cm), were obtained using  $\sigma = (l/A) \cdot (1/R)$ , where *l* is the separator thickness in cm, *A* is the separator cross-sectional area in cm<sup>2</sup> and *R* is the bulk resistance in mΩ. **Interfacial resistance and lithium ion transport numbers (t<sub>Li<sup>+</sup></sub>)** were obtained using the appropriate electrolyte film with symmetric nonblocking lithium electrodes at 60 °C. The interfacial resistance was measured under open circuit potential. The lithium ion transference number was obtained using the modified d.c./a.c., steady-state current method, which contains corrections for slow diffusion coefficients of the ionic species, slow electrode kinetics and passivation films formed on the electrodes:<sup>26</sup>

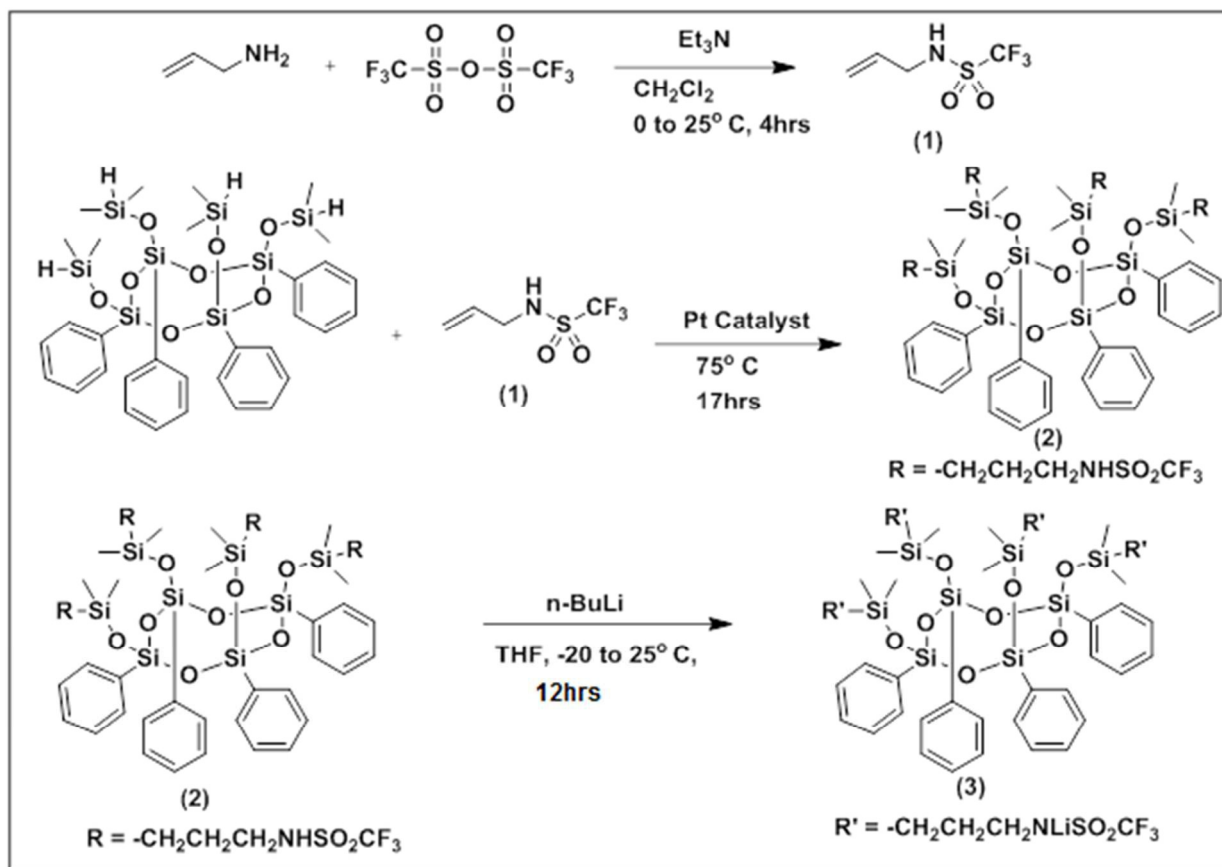
$$t_{Li^+} = I_{ss} (\Delta V - I_o R_o) / I_o (\Delta V - I_s R_{ss})$$

or the same but multiplied by R<sub>ss</sub>/R<sub>o</sub> (however, R<sub>ss</sub> ~ R<sub>o</sub>).<sup>27</sup> A DC pulse (DV) of 10 mV was used to polarize the cell, and the initial current, I<sub>o</sub>, and resistance, R<sub>o</sub> and final, steady state, I<sub>ss</sub>, R<sub>ss</sub> values measured. I<sub>o</sub> originates from the migration of both the anions and cations, while I<sub>ss</sub> is due to the migration of only the cations. Data was fit to the appropriate equivalent circuits using Echem analyst software. **Linear sweep voltammetry** was used to determine the electrochemical stability window of PYR<sub>14</sub>TFSI/MC/4mer-(LiTFSI)<sub>4</sub> = 80/20/0.20M at 60 °C using a stainless steel working electrode and a lithium counter/reference electrode, and the voltage was swept from 0.7 to 7.0 V at a rate of 1 mV s<sup>-1</sup>.

## Materials and Methods

**Synthesis of 4mer-(LiTFSI)<sub>4</sub> = PhSi<sub>4</sub>O<sub>4</sub>[(Si(CH<sub>3</sub>)<sub>2</sub>-R)]<sub>4</sub> with R = -CH<sub>2</sub>CH<sub>2</sub>CH<sub>2</sub>NLiSO<sub>2</sub>CF<sub>3</sub>**

The synthesis of the PhSi<sub>4</sub>O<sub>4</sub>[(Si(CH<sub>3</sub>)<sub>2</sub>-H)]<sub>4</sub> (4mer-(SiH)<sub>4</sub>) has been described previously<sup>40</sup>. The synthesis of PhSi<sub>4</sub>O<sub>4</sub>[(Si(CH<sub>3</sub>)<sub>2</sub>-R)]<sub>4</sub>, R = -CH<sub>2</sub>CH<sub>2</sub>CH<sub>2</sub>NLiSO<sub>2</sub>CF<sub>3</sub> is presented in **Scheme I**. The details of the synthesis of allyltrifluoromethylsulfonamide (**1**), the hydrosilylation of allyltrifluoromethylsulfonamide with 4mer-(SiH)<sub>4</sub> to form PhSi<sub>4</sub>O<sub>4</sub>[(Si(CH<sub>3</sub>)<sub>2</sub>-R)]<sub>4</sub>, R = -CH<sub>2</sub>CH<sub>2</sub>CH<sub>2</sub>NHISO<sub>2</sub>CF<sub>3</sub> (**2**), and the conversion to the lithium salt (**3**) are presented in the **SI** and **Figures S1-S4**.



Reaction Scheme I

### Preparation of $\text{PYR}_{14}\text{TFSI}/\text{MC}/4\text{mer}-(\text{LiTFSI})_4$ and $\text{PYR}_{14}\text{TFSI}/\text{MC}/\text{LiTFSI}$ ion gels

Sample preparation and storage were in a  $\text{N}_2$  or argon purged MBraun glove box. To prepare the  $\text{PYR}_{14}\text{TFSI}/\text{MC}/4\text{mer}-(\text{LiTFSI})_4$  ion-gels, calculated amounts of MC (2 wt/v %), 4mer-(LiTFSI)<sub>4</sub> and  $\text{PYR}_{14}\text{TFSI}$  were co-dissolved in DMSO at room temperature (RT). This solution was left stirring overnight in the glove box and the viscous solution cast on Teflon™ plates. The DMSO was evaporated first at room temperature, then on a hot plate inside the glove box and finally in a vacuum oven at 110–120 °C for ~ 48h to remove residual DMSO; confirmation of removal of residual DMSO was by TGA. The solutions did not gel as observed when DMF was used as the solvent<sup>1</sup>. Instead, the films only became more viscous as the DMSO was removed, until they finally solidified upon complete removal of DMSO. Films with  $\text{PYR}_{14}\text{TFSI}/\text{MC}/4\text{mer}-(\text{LiTFSI})_4 = 60/40/0$ , 70/30/0, 80/20/0, 90/10/0, 60/40/0.20, 70/30/0.20, 80/20/0.20 and 90/10/0.20 were prepared.

For comparison,  $\text{PYR}_{14}\text{TFSI}/\text{MC}/\text{LiTFSI} = 90/10/0.20\text{M}$  ion-gels were prepared by co-dissolution of the constituents in DMF at 90 °C. The liquid solution was cast onto Teflon™ plates in the glove box, which gelled upon cooling<sup>1</sup>, and the DMF was evacuated at room temperature (RT), followed by heat treatment in vacuum at 90 °C to remove residual DMF. The labile proton on DMF did not displace  $\text{Li}^+$  in LiTFSI,

but did so with the 4mer-(LiTFSI)<sub>4</sub>, so DMF could not be used to prepare PYR<sub>14</sub>TFSI/MC/4mer-(LiTFSI)<sub>4</sub> ion-gels.

## Results and Discussion

### **Characterization of 4mer-(LiTFSI)<sub>4</sub>**

It was not possible to obtain a single crystal of the 4mer-(LiTFSI)<sub>4</sub> (**Product 3**), which remained amorphous (**Figure S3**). However, the precursor amide (**Product 2**), although initially a viscous liquid, crystallized after storage in the refrigerator. Both single crystal and powder x-ray diffraction data were obtained (which were distinct from the starting material and did not contain any LiTFSI). The generated powder pattern from the single crystal data agreed well with the experimental powder pattern (**Figure S4**). The images (**Figure 1**) show that the phenyl groups are preferentially on one side of a pancake like structure, held apart by the SiO<sub>1.5</sub> ring, with the NH(SO<sub>2</sub>)-CF<sub>3</sub> groups as far away from each other as possible.

### **Thermal Analysis: TGA and DSC**

Maximum degradation temperatures ( $T_d^{\max}$ ) obtained from the DTGA (**Figure 2, TGA in Figure S5**) are summarized in **Table 1**. The TGA data indicate that the degradation temperatures of the ion gels are all > 300 °C and are determined by the MC component, which has a considerably lower  $T_d^{\max}$  than the PYR<sub>14</sub>TFSI. The major degradation peak for the 4mer-(LiTFSI)<sub>4</sub> ( $T_d = 266$  °C) is lower than for LiTFSI ( $T_d = 400$  °C), and its pattern of thermal degradation is more complex compared with the single degradation peak for the LiTFSI, and is not completely decomposed due to pyrolysis and residual ash of the phenyl groups and SiO<sub>1.5</sub>. (**Figure S6**).

Addition of 0.20M 4mer-(LiTFSI)<sub>4</sub> to PYR<sub>14</sub>TFSI eliminates the  $T_d^{\max}$  of pure 4mer-(LiTFSI)<sub>4</sub> and increases  $T_d^{\max}$  of PYR<sub>14</sub>TFSI by 23 °C (from 452 to 475 °C), indicating that the dissolution of the 4mer-(LiTFSI)<sub>4</sub> in PYR<sub>14</sub>TFSI prevents its degradation at lower temperatures. Increasing addition of MC to PYR<sub>14</sub>TFSI decreases  $T_d^{\max}$  of PYR<sub>14</sub>TFSI by 10 °C (from 452 to 442 °C); this small change is consistent with the immiscibility of MC in PYR<sub>14</sub>TFSI. Addition of MC to PYR<sub>14</sub>TFSI/4mer-(LiTFSI)<sub>4</sub> decreases  $T_d^{\max}$  of PYR<sub>14</sub>TFSI/4mer-(LiTFSI)<sub>4</sub> by 33 °C (from 475 °C to 442 °C). These results suggest that the 4mer-(LiTFSI)<sub>4</sub> makes the MC and PYR<sub>14</sub>TFSI more compatible. The effect on the degradation of MC is that its  $T_d^{\max}$  decreases by an average of 29 °C when mixed with PYR<sub>14</sub>TFSI, and by an average of 12.5 °C when mixed with PYR<sub>14</sub>TFSI/4mer-(LiTFSI)<sub>4</sub> (Note: this lower decrease occurs because PYR<sub>14</sub>TFSI/4mer-(LiTFSI)<sub>4</sub> has a higher initial  $T_d^{\max}$  than PYR<sub>14</sub>TFSI by 23 °C). As discussed below, DSC, DMA and x-ray data suggest that PYR<sub>14</sub>TFSI/MC/4mer-(LiTFSI)<sub>4</sub> is micro-phase separated into regions composed predominantly of PYR<sub>14</sub>TFSI/4mer-(LiTFSI)<sub>4</sub> and regions where the MC fibrils are swollen with PYR<sub>14</sub>TFSI or PYR<sub>14</sub>TFSI/4mer-(LiTFSI)<sub>4</sub>. The swelling of the MC with PYR<sub>14</sub>TFSI or PYR<sub>14</sub>TFSI/4mer-(LiTFSI)<sub>4</sub> may make the MC more accessible to degradation.

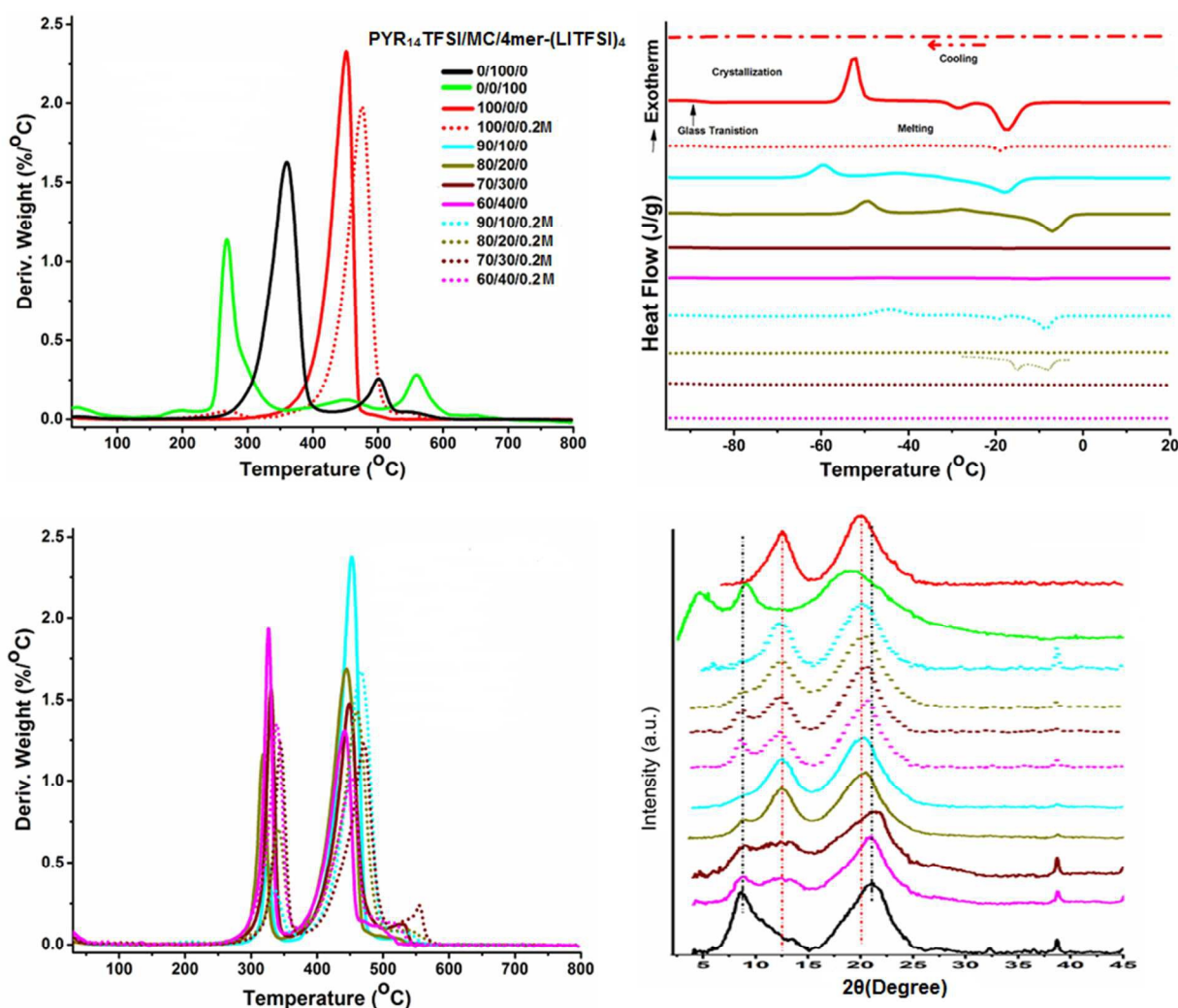


**Figure 2.** Thermal analysis and X-ray diffraction data for 4mer-(LiTFSI)<sub>4</sub>, PYR<sub>14</sub>TFSI/MC and PYR<sub>14</sub>TFSI/MC/0.25M: (i) TGA and DTGA thermograms; (ii) DSC traces of PYR<sub>14</sub>TFSI during heating and cooling and upon addition of MC and MC/0.25M 4mer-(LiTFSI)<sub>4</sub>; 80/20 PYR<sub>14</sub>TFSI/MC/0.25M 4mer-(LiTFSI)<sub>4</sub> expanded 200% to show slight crystallization; (iii) X-ray diffraction data of neat MC, PYR<sub>14</sub>TFSI, 4mer-(LiTFSI)<sub>4</sub> and blends of PYR<sub>14</sub>TFSI/MC/0.25M 4mer-(LiTFSI)<sub>4</sub> at -173 °C.

**Table 1.  $T_d^{\max}$ ,  $T_g$  and X-ray Diffraction Peaks for  $\text{PYR}_{14}\text{TFSI}/\text{MC}/4\text{mer}-(\text{LiTFSI})_4$**

Major $T_d^{\max}$ values and $T_g$ for neat $4\text{mer}-(\text{LiTFSI})_4$ , $\text{PYR}_{14}\text{TFSI}$ , MC and $\text{PYR}_{14}\text{TFSI}/\text{MC}/0.20\text{M } 4\text{mer}-(\text{LiTFSI})_4$ blends							Positions of X-ray diffraction peaks for $\text{PYR}_{14}\text{TFSI}/\text{MC}/4\text{mer}-(\text{LiTFSI})_4$		
Sample	$T_d^{\max}$ ( $^{\circ}\text{C}$ )			$T_g$			Peak 1 ( $^{\circ}$ )	Peak 2 ( $^{\circ}$ )	Peak 3 ( $^{\circ}$ )
	$4\text{mer}-(\text{LiTFSI})_4$	MC	$\text{PYR}_{14}\text{TFSI}$	$\text{PYR}_{14}\text{TFSI}$	MC		MC	$\text{PYR}_{14}\text{TFSI}$	MC or $\text{PYR}_{14}\text{TFSI}$
				DSC	$\tan\delta$	$\tan\delta$			
$\text{PYR}_{14}\text{TFSI}/\text{MC}/4\text{merLiTFSI}$									
0/0/0.20M	266						4.61*	8.91*	19.01*
100/0/0	-		452	-86.6				12.60	20.90
0/100/0	-	353			-63 <sup>†</sup>	201	8.57		21.09
100/0/0.20M	-		475	-83.6					
90/10/0	-	325	452	-85.5		172		12.48	20.31
80/20/0	-	316	448	-84.5	-75	182	8.74	12.60	20.53
70/30/0	-	330	444	-85.2	-69	169	8.86	12.90	21.20
60/40/0	-	325	442	-86.0	-73	184	8.74	12.72	20.88
100/0/0.20M									
90/10/0.20M	-	336	465	-83.2		165		12.32	20.14
80/20/0.20M	-	342	460	-84.2	-71	173	8.50	12.60	20.53
70/30/0.20M	-	344	456	-85.8	-70	176	8.67	12.53	20.59
60/40/0.20M	-	340	453	-85.4	-75	182	8.52	12.42	20.71

\*These are the peaks for  $4\text{merLiTFSI}$ ; <sup>†</sup>secondary transition of MC

DSC data (**Figure 2**) indicate, as previously observed<sup>1, 41</sup>, that the neat  $\text{PYR}_{14}\text{TFSI}$  supercools, and thus crystallizes and remelts upon heating. Addition of 0.20 M  $4\text{mer}-(\text{LiTFSI})_4$  suppresses the crystallization and almost completely suppresses the melt endotherm of  $\text{PYR}_{14}\text{TFSI}$ . When compared with previously reported  $\text{PYR}_{14}\text{TFSI}/\text{LiTFSI}$  data<sup>41</sup>, and similar data obtained here (**SI Figure 7**), the  $4\text{mer}-(\text{LiTFSI})_4$  is more effective at suppressing the  $\text{PYR}_{14}\text{TFSI}$  melt endotherm. Addition of increasing amounts of MC to  $\text{PYR}_{14}\text{TFSI}/0.20\text{M } 4\text{mer}-(\text{LiTFSI})_4$  almost completely suppress crystallization at  $\text{PYR}_{14}\text{TFSI}/\text{MC} < 80/20$  (there is a very small crystallization peak in the 80/20 sample shown as an insert). MC by itself is less effective at the suppression than  $4\text{mer}-(\text{LiTFSI})_4$ . In fact, comparison of  $\text{PYR}_{14}\text{TFSI}/\text{MC}/4\text{mer}-(\text{LiTFSI})_4 = 100/0/0.20\text{M}$  with  $90/10/0.20\text{M}$  shows that the suppression of crystallinity is more effective without the MC. This suggests that there may be competition/sharing of the  $4\text{mer}-(\text{LiTFSI})_4$  between the MC and  $\text{PYR}_{14}\text{TFSI}$ , so that in the mixed (90/10/0.20M) system there is less  $4\text{mer}-(\text{LiTFSI})_4$  to disrupt  $\text{PYR}_{14}\text{TFSI}$  crystallization.

The expanded DSC data at low temperature (**Figure S8** and **Table 1**) show that  $T_g$  of the  $\text{PYR}_{14}\text{TFSI}$  increases from  $-86.6\text{ }^\circ\text{C}$  to  $-83.6\text{ }^\circ\text{C}$  with addition of  $0.20\text{M}$   $4\text{mer}-(\text{LiTFSI})_4$ , and that separate addition of MC to  $\text{PYR}_{14}\text{TFSI}$  increases the  $T_g$  by a smaller amount ( $\sim 1\text{ }^\circ\text{C}$ ), to an average of  $-85.3\text{ }^\circ\text{C}$ . Addition of both MC and  $0.20\text{ M}$   $4\text{mer}-(\text{LiTFSI})_4$  increases  $T_g$  monotonically to  $-85.4\text{ }^\circ\text{C}$ . Although these  $T_g$  effects are small, they indicate that the  $4\text{mer}-(\text{LiTFSI})_4$  has a greater interaction with the  $\text{PYR}_{14}\text{TFSI}$  than does the MC, as might be expected, since the  $4\text{mer}-(\text{LiTFSI})_4$  is actually dissolved in the  $\text{PYR}_{14}\text{TFSI}$ , while MC and  $\text{PYR}_{14}\text{TFSI}$  are not miscible.

### X-ray diffraction

X-ray diffraction data (**Figure 2**, **Table 1**) indicate that  $\text{PYR}_{14}\text{TFSI}/\text{MC}/4\text{mer}-(\text{LiTFSI})_4$  ion gels are phase separated. The  $4\text{mer}-(\text{LiTFSI})_4$  is incorporated at such low concentration ( $0.20\text{ M}$ ) that its x-ray signature (amorphous, since it is dissolved) could not be observed in the blends. The MC has two diffraction peaks at  $8.57^\circ$  and  $21.09^\circ$  (vertical lines  $-\bullet-\bullet-$  are guides to the eye)<sup>1</sup>. The  $8.57^\circ$  peak is separate from the  $\text{PYR}_{14}\text{TFSI}$  peak and thus can be used to observe the persistence of the MC semi-crystalline regions for all the compositions, with and without  $4\text{mer}-(\text{LiTFSI})_4$ , although with decreasing intensity as its percentage in the blends decreases.  $\text{PYR}_{14}\text{TFSI}$  exhibits two broad peaks at  $12.6^\circ$  and  $20.9^\circ$  (vertical  $\bullet\bullet\bullet$  lines are guides to the eye). The  $12.6^\circ$  peak is isolated from any MC peaks and its relative intensity increases compared with the  $8.57^\circ$  peak of MC as its percentage in the blends increases. Although the  $21.09^\circ$  and  $20.9^\circ$  peaks of MC and  $\text{PYR}_{14}\text{TFSI}$  are close, there is a shift in the peak maxima towards  $21.09^\circ$  upon increased MC content in the blends. The persistence of the separate MC and  $\text{PYR}_{14}\text{TFSI}$  (with or without  $0.20\text{M}$   $4\text{mer}-(\text{LiTFSI})_4$ ) peaks in the x-ray diffraction data indicate that there is phase separation in the  $\text{PYR}_{14}\text{TFSI}/\text{MC}/4\text{mer}-(\text{LiTFSI})_4$  ion-gels. This is confirmed by x-ray diffraction data for samples cooled to  $-100\text{ }^\circ\text{C}$ , heated to  $-40\text{ }^\circ\text{C}$  (**Figure S9**), so that the  $\text{PYR}_{14}\text{TFSI}$  crystallinity is maintained and observed clearly as a separate phase in the ion-gels.

### Mechanical Property Data

Tan  $\delta$  data (**Figure 3**, **Table 1**) show that the low temperature glass transition for  $\text{PYR}_{14}\text{TFSI}$  or  $\text{PYR}_{14}\text{TFSI}/0.20\text{M}$   $4\text{mer}-(\text{LiTFSI})_4$  in the blends with MC occurs at  $\langle -72\text{ }^\circ\text{C} \rangle$  for samples with and without  $4\text{mer}-(\text{LiTFSI})_4$ , which is not unexpected since there was very little shift observed by DSC (**Table 1**, **Figure S8**,  $T_g \sim -85\text{ }^\circ\text{C}$ ). This strongly suggests that the  $\text{PYR}_{14}\text{TFSI}$  and  $\text{PYR}_{14}\text{TFSI}/4\text{mer}-(\text{LiTFSI})_4$  is phase separated in these ion-gels. Previously, we prepared  $\text{PYR}_{14}\text{TFSI}/\text{MC}$  ion-gels from DMF, which gelled upon cooling, and where the DMF was removed from the gel at RT. In that work,  $T_g$  of the  $\text{PYR}_{14}\text{TFSI}$  also did not shift from its neat value<sup>1</sup>. The  $T_g$  of MC in the ion-gel was also the same as the  $T_g$  of neat MC<sup>1</sup>. However, in the  $\text{PYR}_{14}\text{TFSI}/\text{MC}$  blends cast from DMSO (which did not gel upon cooling) the  $T_g$  of MC decreases from its value of  $201\text{ }^\circ\text{C}$  to lower values that decrease with increasing  $\text{PYR}_{14}\text{TFSI}$  content. This shift to lower temperatures is slightly greater in the  $\text{PYR}_{14}\text{TFSI}/\text{MC}/4\text{mer}-(\text{LiTFSI})_4$  blends, suggesting that the  $4\text{mer}-(\text{LiTFSI})_4$  increases the compatibility/interactions of the components. Thus, although the bulk of the  $\text{PYR}_{14}\text{TFSI}/4\text{mer}-(\text{LiTFSI})_4$  is in a separate phase (as observed by the separate  $T_g$  of the  $\text{PYR}_{14}\text{TFSI}/4\text{mer}-(\text{LiTFSI})_4$  in the DSC and tan  $\delta$  data (**Table 1**), the MC is affected by the presence of  $\text{PYR}_{14}\text{TFSI}/4\text{mer}-(\text{LiTFSI})_4$ , as manifest by its reduced  $T_g$ . We suggest that this results from swelling of the MC fibrils<sup>42</sup> with the  $\text{PYR}_{14}\text{TFSI}$  or  $\text{PYR}_{14}\text{TFSI}/4\text{mer}-(\text{LiTFSI})_4$ . As

discussed below, the presence of lithium salt can increase the compatibility of the MC and  $\text{PYR}_{14}\text{TFSI}$  (and thus lower the  $T_g$  of the MC).

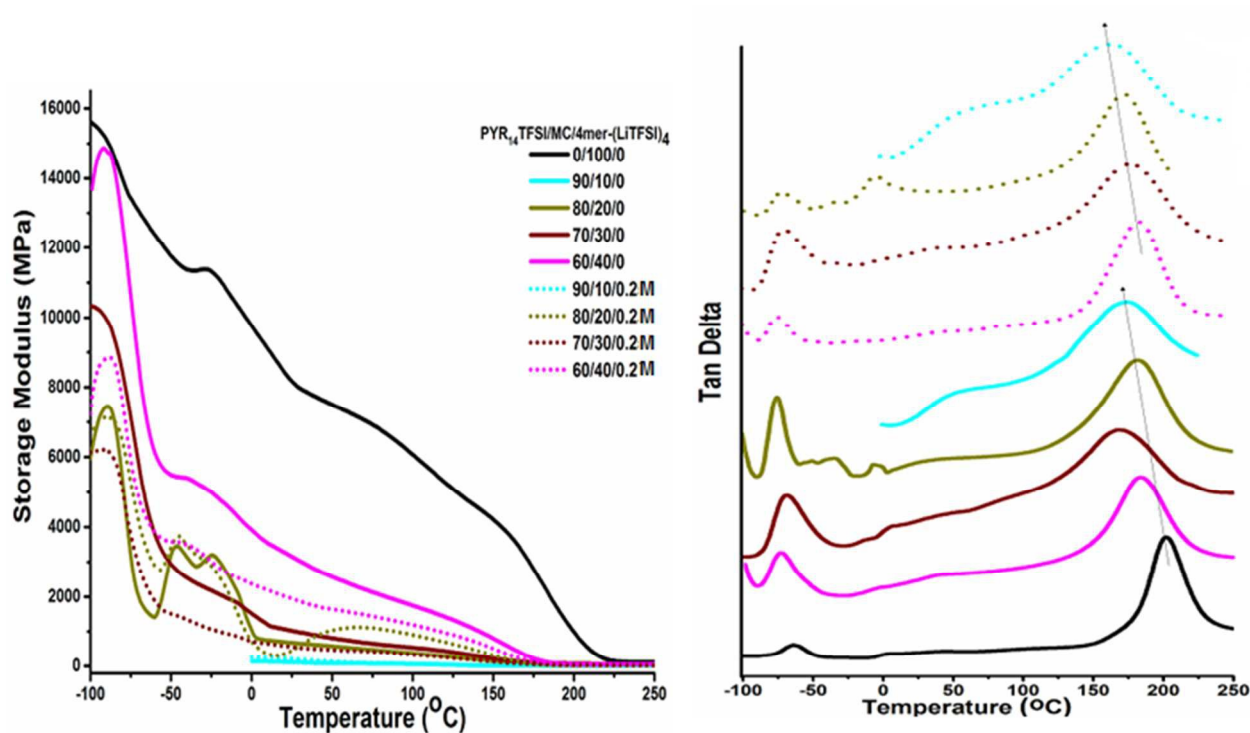


**Figure 3.** Tan  $\delta$  and storage modulus data. For the 80/20 composition, the crystallization and melt of the 4mer-(LiTFSI)<sub>4</sub> (as also seen in the DSC, **Figure 2**) can be observed. The peak at  $-63^\circ\text{C}$  may be due to a secondary relaxation in MC<sup>1</sup>.

Storage moduli data (**Figure 3**) for the blends show as expected that addition of increasing amounts of the  $\text{PYR}_{14}\text{TFSI}$  ionic liquid to the MC decreases the moduli of the blends. When 0.20 M 4mer-(LiTFSI)<sub>4</sub> is added (seen more clearly in the 60/40 and 7/30 compositions), the moduli with salt are decreased compared with the blends without 4mer-(LiTFSI)<sub>4</sub>. Since the moduli are determined by the MC component, the swelling of the MC fibrils (as observed by the decreased MC  $T_g$  when 0.20 M 4mer-(LiTFSI)<sub>4</sub> was added to the  $\text{PYR}_{14}\text{TFSI}$ ) also accounts for the drop in moduli with added salt. For all compositions, there is a drop-off in the storage moduli at  $T_g$  of the MC. However, the moduli remain in the MPa range to temperatures of  $150^\circ\text{C}$  as tabulated in **Table 2**. This is in contrast with the rubbery mechanical properties found for many ion gels, e.g. RTILs gelled with silica NPs<sup>33</sup>.

**Table 2. Conductivity ( $\sigma$ ), modulus ( $E'$ ) and lithium ion transference number ( $t_{Li^+}$ ) as a function to  $PYR_{14}TFSI/MC/4mer-(LiTFSI)_4$  composition**

Sample	$\sigma$ mS/cm 30 <sup>o</sup> C	$E'$ MPa 30 <sup>o</sup> C	$\sigma$ mS/cm 60 <sup>o</sup> C	$t_{Li^+}$	$E'$ MPa 60 <sup>o</sup> C	$\sigma$ mS/cm 90 <sup>o</sup> C	$E'$ MPa 90 <sup>o</sup> C	$E'$ MPa 150 <sup>o</sup> C
0/100/0		7973			7298		6446	4213
60/40/0	0.04	3027	0.14		2398	0.45	1888	775
70/30/0	0.12	975	0.3		740	0.57	579	224
80/20/0	1.0	654	1.6		533	2.9	414	148
90/10/0	1.3	109	3.2		81	5.6	69	14
100/0/0	4.3		9.8			15.5		
60/40/0.20M	0.005	1884	0.006	0.39	1568	0.008	1283	464
70/30/0.20M	0.09	590	0.19	0.36	447	0.33	367	128
80/20/0.20M	0.3	570	0.7	0.35	1107	1.4	985	312
90/10/0.20M	0.6	198	1.3	0.19	115	1.9	76	17
100/0/0.20	3.3		7.5	0.09		11.4		

### Electrochemical Data

Conductivity data (**Figure 4** and **Table 2**) show, as previously observed, that the conductivity decreases with addition of lithium salt (here 4mer-(LiTFSI)<sub>4</sub>) and with increasing amount of MC in the blends<sup>1</sup>. Addition of 0.20M 4mer-(LiTFSI)<sub>4</sub> to pure PYR<sub>14</sub>TFSI has minimal effect on the conductivity. This has been attributed, in other LiX/RTILs, to the small contribution of the LiX ions to the total number of ions in the solution<sup>43</sup>. Addition of MC to PYR<sub>14</sub>TFSI or MC to PYR<sub>14</sub>TFSI/0.20M 4mer-(LiTFSI)<sub>4</sub> results in much greater reductions (by > 1 order of magnitude) in conductivity compared with addition of 0.20M 4mer-(LiTFSI)<sub>4</sub> to PYR<sub>14</sub>TFSI.

Mixtures of PYR<sub>14</sub>TFSI/MC/LiTFSI and PYR<sub>14</sub>TFSI/MC/4mer-(LiTFSI)<sub>4</sub> at the same molarity (0.20 M Li<sup>+</sup>) and MC composition have similar ionic conductivity (**Figure S10**). In single ion conductors (SICs), low ionic conductivities have been attributed to ion aggregation, much greater than observed in the case of the corresponding LiX anions. Here, the similar conductivities for LiTFSI and 4mer-(LiTFSI)<sub>4</sub> in the ion gels indicate that whatever ion pairing occurs is the same for both salts. Unlike SICs in which the pendant anion is attached to a flexible polymer backbone, so that ionic aggregation can occur, here the anions are attached to a rigid SiO<sub>1.5</sub> structure (**Figure 1**) that inhibits this type of association.

The stability window (**Figure 4**), measured for PYR<sub>14</sub>TFSI/MC/4mer-(LiTFSI)<sub>4</sub> = 80/20/0.20M using a stainless steel working electrode and lithium as the counter and reference electrodes was 0.8V to 5V, with a threshold current of 50  $\mu$ ampere/cm<sup>2</sup>. This is above the 4V stability range necessary in practical LIBs, although less than previously reported for battery grade PYR<sub>14</sub>TFSI (~ 6V)<sup>6</sup>, with little degradation observed due to the MC or 4mer-(LiTFSI)<sub>4</sub>. The interfacial resistance (**Figure 4**) increases for the first 36 hours, decreases until 89 hours and then stabilizes at 89 hours, which was further confirmed at 160 hours (not shown). These trends are often observed as the SEI layer on Li metal is formed, partially dissolves and stabilizes; no attempt was made to investigate the composition of the SEI.

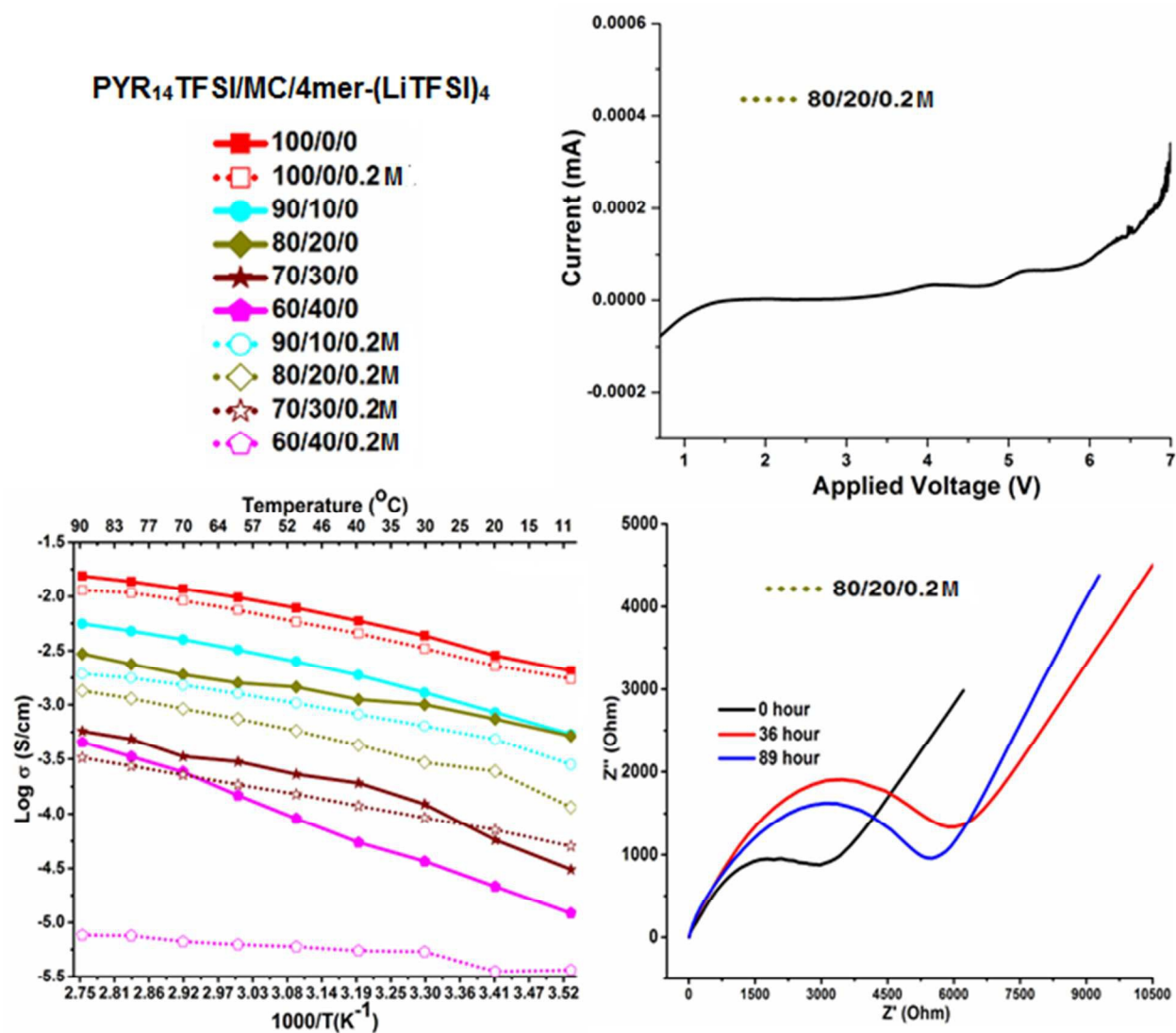


**Figure 4.** Conductivity versus  $1000/T$  (K<sup>-1</sup>) for PYR<sub>14</sub>TFSI/MC/4mer-(LiTFSI)<sub>4</sub> as a function of composition; Electrochemical stability window and interfacial resistance (at 60 °C) for PYR<sub>14</sub>TFSI/MC/4mer-(LiTFSI)<sub>4</sub> = 80/20/0.25M

Lithium ion transference numbers (**Table 2**) were similar for PYR<sub>14</sub>TFSI/4mer-(LiTFSI)<sub>4</sub> ( $t_{Li^+} = 0.09$ ) and PYR<sub>14</sub>TFSI/LiTFSI ( $t_{Li^+} = 0.1$ ) (**Table S1**) at 0.20M LiX. The value of  $t_{Li^+}$  obtained for 0.20M LiTFSI in PYR<sub>14</sub>TFSI was slightly higher than that measured by PFG-NMR ( $t_{Li^+} \sim 0.07$ )<sup>18</sup>. Reported values of  $t_{Li^+}$  for RTIL/LiX pairs, from PFG-NMR (where the individual self-diffusion coefficients of the anions and cations are measured)<sup>7, 10, 12, 18</sup> or dc polarization<sup>21, 30, 44</sup> (using Li metal as non-blocking electrodes<sup>45, 46</sup>) methods are in the range of  $t_{Li^+} = 0.023$  to  $0.132$ <sup>7, 10, 12, 18</sup>. Larger anions with greater charge delocalization such as 4mer-(TFSI)<sub>4</sub> or TFSI enhance  $t_{Li^+}$  by decreasing ion pairs and aggregates,

thus leading to higher lithium ion diffusivities. Although increased molarity of LiX in RTILs can increase  $t_{\text{Li}^+}$ , this was not possible for  $\text{PYR}_{14}\text{TFSI}/4\text{mer}-(\text{LiTFSI})_4$ , since solubility problems were observed at 0.5M  $4\text{mer}-(\text{LiTFSI})_4$ .

With addition of MC,  $t_{\text{Li}^+}$  increased and levelled off at  $t_{\text{Li}^+} \sim 0.36$  for  $\text{PYR}_{14}\text{TFSI}/\text{MC}/4\text{mer}-(\text{LiTFSI})_4 = 80/20/0.20\text{M}$ . In the case of  $\text{PYR}_{14}\text{TFSI}/\text{MC}/\text{LiTFSI} = 80/20/0.20\text{M}$ ,  $t_{\text{Li}^+} = 0.18$ , half that of the  $4\text{mer}-(\text{LiTFSI})_4$  (Table S1). Since the  $t_{\text{Li}^+}$  values were similar in the neat liquids, this suggests that the interactions of  $4\text{mer}-(\text{TFSI})_4$  anions or the TFSI<sup>-</sup> anions of  $\text{PYR}_{14}\text{TFSI}$  with the MC play a role in retarding migration of the anions, effectively increasing  $t_{\text{Li}^+}$ , and further that the interaction is greater for the  $4\text{mer}-(\text{TFSI})_4$ . Polymers have previously been observed to increase  $t_{\text{Li}^+}$  by interacting with the anions, slowing their motions, and decreasing anion interactions with the Li ions, thus increasing the number of free  $\text{Li}^+$  available for conduction. For the  $\text{PYR}_{14}\text{TFSI}/0.20\text{M LiTFSI}$  investigated here, indirect evidence of interactions between the components is suggested by the DSC, DMA and X-ray diffraction data. In addition, cellulose solubility studies shed some insight on the interactions that occur in these systems.

Studies of cellulose indicate that dissolution depends on the ability of solvents to disrupt the intra- and inter-molecular hydrogen bond network<sup>47</sup> and the hydrophobic interactions between cellulose molecules<sup>48</sup>. Cellulose is regarded as amphiphilic, with the equatorial direction of the D-glucopyranose ring having a hydrophilic character (since all three OH groups are located on the equatorial position of the ring) and the axial direction have a hydrophobic character (since the C-H hydrogens are located on the axial positions of the ring). Further, dimethyl acetamide/LiCl (DMAc/LiCl) is a well-known mixed inorganic/organic solvent for cellulose<sup>49</sup>. The mechanism of solubility of cellulose in LiCl/DMAc is not fully understood, but it is believed that the lithium ions are linked with the carbonyl of DMAc. The Cl<sup>-</sup> anion (due to its basicity) then interferes with the inter- and intra-hydrogen bonds in cellulose, possibly complexing three OH groups of cellulose<sup>50</sup>, and resulting in an anionically charged polymer, with [Li-DMAc] as the counterion, followed by the exchange of DMAc in the lithium coordination sphere by cellulose hydroxyl groups. This polyelectrolyte effect is also observed in the tetra-n-butylammonium fluoride (TBAF)/DMSO system, where F<sup>-</sup> binds to the cellulose and expands the chain due to charge repulsion and NMR evidence indicates that the F<sup>-</sup> act as hydrogen bond acceptors of the cellulose OH groups<sup>51</sup>. In general, small, strong polarizing cations (e.g.  $\text{Li}^+$ ) and large polarizable anions are found to interact strongly with cellulose. <sup>7</sup>Li NMR evidence supports the direct interaction between Li and cellulose hydroxyl groups<sup>52</sup>, while large polarizable anions are effectively hydrophobic and are enriched at the hydrophobic surface of cellulose.

Although these results have been obtained for cellulose, analogies can be made with MC, since the axial plane is still “hydrophobic” and the equatorial plane contains fewer OH groups and thus less intra- and inter- molecular hydrogen bonding (1.6-1.9 of the (equatorial) OH are substituted with methyl groups). In the case of  $\text{PYR}_{14}\text{TFSI}/\text{MC}/4\text{mer}-(\text{LiTFSI})_4$  in DMSO, by analogy with the LiCl/DMAc, the  $\text{Li}^+$  would initially be bound with the carbonyl of DMSO, leaving the large, polarizable  $4\text{mer}-(\text{TFSI})_4$  or TFSI<sup>-</sup> anions to hydrogen bond with any free OH groups on MC or interact with them by hydrophobic association. Lewis acid-base interactions between surface (OH) sites on inorganic fillers incorporated into RTILs with the X<sup>-</sup> anions of the lithium salt have also been shown to increase the fraction of  $\text{Li}^+$  cations available for conduction, as observed for silica ( $\text{SiO}_2$ )<sup>30</sup> ( $t_{\text{Li}^+} = 0.1- 0.27$ ), polyhedral oligomeric silsesquioxanes (POSS) with hydroxyl groups (POSS-OH)<sup>53</sup> ( $t_{\text{Li}^+} = 0.20- 0.49$ ), and  $\text{TiO}_2$  nanotubes<sup>44</sup> ( $t_{\text{Li}^+}$

= 0.295, 0.459). The large, bulky 1-butyl-1-methylpyrrolidinium ( $\text{PYR}_{14}^+$ ) cation will not have easy access (steric restrictions) to the O of the cellulose hydroxyls, as these cations have been shown to only weakly coordinate to the anions due to the steric shielding of the positive charge<sup>54</sup>. It is worth noting that the pyrrolidinium cation is not one that dissolves cellulose<sup>47</sup>.

The smaller  $\text{Li}^+$  ion on the other hand, can have access to the hydroxyls, which become part of the  $\text{Li}^+$  ion coordination shell with DMSO (which is eventually completely removed), weakening the association of  $\text{Li}^+$  to 4mer-(TFSI)<sub>4</sub> or TFSI. In PEO/ $\text{PYR}_{14}$ TFSI/LiTFSI polymer electrolytes, Raman data suggest that there is mixed  $\text{Li}^+$  coordination to both PEO and TFSI<sup>55</sup> and for the cationic polymeric ionic liquid (PIL), poly(diallyldimethylammonium bis(trifluoromethyl) sulfonyl imide) (PDADMATFSI), the polymer also was shown to interact with the anion coordination shell, reducing  $\text{Li}^+$  ion-TFSI anion interactions<sup>56</sup>.

The  $\text{PYR}_{14}$ TFSI/MC/0.20M 4mer-(LiTFSI)<sub>4</sub> ion gels thus have both high  $t_{\text{Li}^+}$  and high ionic conductivities, which is unusual for RTIL ion gels. In the case of PEO/BMPyTFSI/LiTFSI (BMPyTFSI = 1-butyl-4-methylpyridinium bis(trifluoromethanesulfonyl)imide),  $t_{\text{Li}^+}$  was found to decrease and ionic conductivity to increase with increasing mole fraction of the ionic liquid<sup>43</sup>. While values of  $t_{\text{Li}^+}$  were high, conductivities ( $\sigma$ ) were low, e.g.  $t_{\text{Li}^+} = 0.363$ ,  $\sigma = 2.1 \times 10^{-6}$  S/cm to  $t_{\text{Li}^+} = 0.150$ ,  $\sigma = 6.9 \times 10^{-5}$  S/cm. In  $\text{P}_{13}$ TFSI/LiTFSI/PVDV-HFP ( $\text{P}_{13}$ TFSI = 1-methyl-3-propylpyrrolidinium bis(trifluoromethanesulfonyl)imide, PVDF-HFP = poly(vinylidene-co-hexafluoropropylene),  $t_{\text{Li}^+}$  are low ( $t_{\text{Li}^+} = 0.034$  at 1M LiTFSI)<sup>57</sup>. In the case of cationic ILs tethered to  $\text{ZrO}_2$  nanoparticles, addition of LiTFSI resulted in a large  $t_{\text{Li}^+}$  of 0.35, possibly due to immobilization of the IL cations by the  $\text{ZrO}_2$  nanoparticle core, which decreases their contribution to the ionic conduction (as well as increasing the ionic conductivity), but conductivities were again low ( $10^{-5}$  S/cm)<sup>58</sup>.

A final comment is that in single ion conductors (SICs), low ionic conductivities have been attributed to ion aggregation, much greater than observed in the case of the corresponding LiX anions. Here, the conductivities are the same for neat LiTFSI and the 4mer-(LiTFSI)<sub>4</sub>, indicating that whatever ion pairing occurs is the same for both salts. Unlike SICs in which the pendant anion is attached to a flexible polymer backbone, so that ionic aggregates can occur, here the anions are attached to a rigid structure, the  $\text{SiO}_{1.5}$  cage (**Figure 1**) that prevents this type of association.

## Conclusions

Blends of 4mer-(LiTFSI)<sub>4</sub> can be formulated into ion-gel electrolytes by co-dissolution with MC and  $\text{PYR}_{14}$ TFSI in DMSO and evaporation of the DMSO. The DSC, X-ray diffraction and DMA data suggest that the ion gels are micro-phase separated into a  $\text{PYR}_{14}$ TFSI/4mer-(LiTFSI)<sub>4</sub> rich phase and a semicrystalline MC phase swollen with  $\text{PYR}_{14}$ TFSI/4mer-(LiTFSI)<sub>4</sub> that decreases its  $T_g$ . What is interesting about these materials is that both ionic conductivity and lithium ion transference numbers can be simultaneously enhanced while maintaining structurally strong films with moduli in the MPa range. The  $\text{PYR}_{14}$ TFSI/MC/0.20M 4mer-(LiTFSI)<sub>4</sub> ion gels had combined high RT ionic conductivities ( $> 10^{-4}$  S/cm) and transference numbers ( $t_{\text{Li}^+} = 0.35$ ). At the same  $\text{Li}^+$  molarity, ion gels prepared with either LiTFSI or 4mer-(LiTFSI)<sub>4</sub> have very similar conductivities. Unlike what is sometimes observed in the case of single ion conductors, the conductivity does not decrease as the  $t_{\text{Li}^+}$  increases. However, the 4mer-(LiTFSI)<sub>4</sub>, with its large (1242 g/mol) anion, has  $t_{\text{Li}^+}$ 's that are factors of 2 greater than the LiTFSI ( $t_{\text{Li}^+} =$

0.18), so that a greater fraction of the charge is carried by the  $\text{Li}^+$  cation rather than the anion. By analogy with cellulose solubility studies, we propose that this is due to hydrophobic/H-bonding interactions of the 4mer-(TFSI)<sub>4</sub> anion with MC as well as hydrogen bonding of  $\text{Li}^+$  with the OH of MC and thus participation of the MC in the solvation sphere of  $\text{Li}^+$ . The separators have high thermal stability, dictated by the degradation temperature of the MC and the selected Li salt, since the thermal decomposition of the  $\text{PYR}_{14}\text{TFSI}$  is  $> 400$  °C. They also have excellent mechanical properties, with RT moduli,  $E' > 100$  MPa for  $T < 125$  °C, which contrasts with the rubbery mechanical properties found for many ion gels.

### Acknowledgements

Financial support through NSF grants NSF DMR 1207221 and CBET 1437814 is gratefully acknowledged.

### Author Information

Corresponding Author

\*E-mail: slwunder@temple.edu

### Notes

The authors declare no competing financial interest.

### References

1. Mantravadi, R.; Chinnam, P. R.; Dikin, D. A.; Wunder, S. L., High conductivity, high strength solid electrolytes formed by in situ encapsulation of ionic liquids in nanofibrillar methyl cellulose networks. *ACS Appl. Mater. Interfaces* **2016**, am-2016-02903f, (DOI: 10.1021/acsami.6b02903).
2. Lewandowski, A.; Swiderska-Mocek, A., Ionic liquids as electrolytes for Li-ion batteries-An overview of electrochemical studies. *Journal of Power Sources* **2009**, *194*, (2), 601-609.
3. Seki, S.; Ohno, Y.; Kobayashi, Y.; Miyashiro, H.; Usami, A.; Mita, Y.; Tokuda, H.; Watanabe, M.; Hayamizu, K.; Tsuzuki, S.; Hattori, M.; Terada, N., Imidazolium-based room-temperature ionic liquid for lithium secondary batteries - Effects of lithium salt concentration. *Journal of the Electrochemical Society* **2007**, *154*, (3), A173-A177.
4. Seki, S.; Ohno, Y.; Miyashiro, H.; Kobayashi, Y.; Usami, A.; Mita, Y.; Terada, N.; Hayamizu, K.; Tsuzuki, S.; Watanabe, M., Quaternary ammonium room-temperature ionic liquid/lithium salt binary electrolytes: Electrochemical study. *Journal of the Electrochemical Society* **2008**, *155*, (6), A421-A427.
5. Sugimoto, T.; Atsumi, Y.; Kikuta, M.; Ishiko, E.; Kono, M.; Ishikawa, M., Ionic liquid electrolyte systems based on bis(fluorosulfonyl)imide for lithium-ion batteries. *Journal of Power Sources* **2009**, *189*, (1), 802-805.
6. Galinski, M.; Lewandowski, A.; Stepniak, I., Ionic liquids as electrolytes. *Electrochimica Acta* **2006**, *51*, (26), 5567-5580.
7. Hayamizu, K.; Aihara, Y.; Nakagawa, H.; Nukuda, T.; Price, W. S., Ionic conduction and ion diffusion in binary room-temperature ionic liquids composed of emim BF<sub>4</sub> and LiBF<sub>4</sub>. *Journal of Physical Chemistry B* **2004**, *108*, (50), 19527-19532.
8. Takada, A.; Imaichi, K.; Kagawa, T.; Takahashi, Y., Abnormal viscosity increment observed for an ionic liquid by dissolving lithium chloride. *Journal of Physical Chemistry B* **2008**, *112*, (32), 9660-9662.
9. Rosol, Z. P.; German, N. J.; Gross, S. M., Solubility, ionic conductivity and viscosity of lithium salts in room temperature ionic liquids. *Green Chemistry* **2009**, *11*, (9), 1453-1457.

10. Fromling, T.; Kunze, M.; Schonhoff, M.; Sundermeyer, J.; Roling, B., Enhanced Lithium Transference Numbers in Ionic Liquid Electrolytes. *Journal of Physical Chemistry B* **2008**, *112*, (41), 12985-12990.
11. Borodin, O.; Smith, G. D.; Henderson, W., Li<sup>+</sup> cation environment, transport, and mechanical properties of the LiTFSI doped N-methyl-N-alkylpyrrolidinium +TFSI<sup>-</sup> ionic liquids. *Journal of Physical Chemistry B* **2006**, *110*, (34), 16879-16886.
12. Saito, Y.; Umecky, T.; Niwa, J.; Sakai, T.; Maeda, S., Existing condition and migration property of ions in lithium electrolytes with ionic liquid solvent. *Journal of Physical Chemistry B* **2007**, *111*, (40), 11794-11802.
13. Umebayashi, Y.; Harnano, H.; Seki, S.; Minofar, B.; Fujii, K.; Hayamizu, K.; Tsuzuki, S.; Kameda, Y.; Kohara, S.; Watanabe, M., Liquid Structure of and Li<sup>+</sup> Ion Solvation in Bis(trifluoromethanesulfonyl)amide Based Ionic Liquids Composed of 1-Ethyl-3-methylimidazolium and N-Methyl-N-propylpyrrolidinium Cations. *Journal of Physical Chemistry B* **2011**, *115*, (42), 12179-12191.
14. Angenendt, K.; Johansson, P., Ionic Liquid Based Lithium Battery Electrolytes: Charge Carriers and Interactions Derived by Density Functional Theory Calculations. *Journal of Physical Chemistry B* **2011**, *115*, (24), 7808-7813.
15. Castiglione, F.; Famulari, A.; Raos, G.; Meille, S. V.; Mele, A.; Appetecchi, G. B.; Passerini, S., Pyrrolidinium-Based Ionic Liquids Doped with Lithium Salts: How Does Li<sup>+</sup> Coordination Affect Its Diffusivity? *Journal of Physical Chemistry B* **2014**, *118*, (47), 13679-13688.
16. Castiglione, F.; Ragg, E.; Mele, A.; Appetecchi, G. B.; Montanino, M.; Passerini, S., Molecular Environment and Enhanced Diffusivity of Li<sup>+</sup> Ions in Lithium-Salt-Doped Ionic Liquid Electrolytes. *J. Phys. Chem. Lett.* **2011**, *2*, (3), 153-157.
17. Lesch, V.; Jeremias, S.; Moretti, A.; Passerini, S.; Heuer, A.; Borodin, O., A Combined Theoretical and Experimental Study of the Influence of Different Anion Ratios on Lithium Ion Dynamics in Ionic Liquids. *Journal of Physical Chemistry B* **2014**, *118*, (26), 7367-7375.
18. Jeremias, S.; Kunze, M.; Passerini, S.; Schoenhoff, M., Polymerizable Ionic Liquid with State of the Art Transport Properties. *Journal of Physical Chemistry B* **2013**, *117*, (36), 10596-10602.
19. Nicotera, I.; Oliviero, C.; Henderson, W. A.; Appetecchi, G. B.; Passerini, S., NMR investigation of ionic liquid-LiX mixtures: Pyrrolidinium cations and TFSI<sup>-</sup> anions. *Journal of Physical Chemistry B* **2005**, *109*, (48), 22814-22819.
20. Castiglione, F.; Moreno, M.; Raos, G.; Famulari, A.; Mele, A.; Appetecchi, G. B.; Passerini, S., Structural Organization and Transport Properties of Novel Pyrrolidinium-Based Ionic Liquids with Perfluoroalkyl Sulfonylimide Anions. *Journal of Physical Chemistry B* **2009**, *113*, (31), 10750-10759.
21. Kim, J.-K.; Niedzicki, L.; Scheers, J.; Shin, C.-R.; Lim, D.-H.; Wiczorek, W.; Johansson, P.; Ahn, J.-H.; Matic, A.; Jacobsson, P., Characterization of N-butyl-N-methyl-pyrrolidinium bis(trifluoromethanesulfonyl)imide-based polymer electrolytes for high safety lithium batteries. *Journal of Power Sources* **2013**, *224*, 93-98.
22. Bayley, P. M.; Lane, G. H.; Rocher, N. M.; Clare, B. R.; Best, A. S.; MacFarlane, D. R.; Forsyth, M., Transport properties of ionic liquid electrolytes with organic diluents. *Physical Chemistry Chemical Physics* **2009**, *11*, (33), 7202-7208.
23. Bayley, P. M.; Best, A. S.; MacFarlane, D. R.; Forsyth, M., Transport Properties and Phase Behaviour in Binary and Ternary Ionic Liquid Electrolyte Systems of Interest in Lithium Batteries. *Chemphyschem* **2011**, *12*, (4), 823-827.
24. Deshpande, A.; Kariyawasam, L.; Dutta, P.; Banerjee, S., Enhancement of Lithium Ion Mobility in Ionic Liquid Electrolytes in Presence of Additives. *Journal of Physical Chemistry C* **2013**, *117*, (48), 25343-25351.

25. Shin, J. H.; Henderson, W. A.; Tizzani, C.; Passerini, S.; Jeong, S. S.; Kim, K. W., Characterization of solvent-free polymer electrolytes consisting of ternary PEO-LiTFSI-PYR14 TFSI. *Journal of the Electrochemical Society* **2006**, 153, (9), A1649-A1654.
26. Zhu, C. B.; Cheng, H.; Yang, Y., Electrochemical characterization of two types of PEO-based polymer electrolytes with room-temperature ionic liquids. *Journal of the Electrochemical Society* **2008**, 155, (8), A569-A575.
27. Shin, J. H.; Henderson, W. A.; Passerini, S., Ionic liquids to the rescue? Overcoming the ionic conductivity limitations of polymer electrolytes. *Electrochemistry Communications* **2003**, 5, (12), 1016-1020.
28. Shin, J. H.; Henderson, W. A.; Appetecchi, G. B.; Alessandrini, E.; Passerini, S., Recent developments in the ENEA lithium metal battery project. *Electrochimica Acta* **2005**, 50, (19), 3859-3865.
29. Bansal, D.; Cassel, F.; Croce, F.; Hendrickson, M.; Plichta, E.; Salomon, M., Conductivities and transport properties of gelled electrolytes with and without an ionic liquid for Li and Li-ion batteries. *Journal of Physical Chemistry B* **2005**, 109, (10), 4492-4496.
30. Ferrari, S.; Quartarone, E.; Mustarelli, P.; Magistris, A.; Fagnoni, M.; Protti, S.; Gerbaldi, C.; Spinella, A., Lithium ion conducting PVdF-HFP composite gel electrolytes based on N-methoxyethyl-N-methylpyrrolidinium bis(trifluoromethanesulfonyl)-imide ionic liquid. *Journal of Power Sources* **2010**, 195, (2), 559-566.
31. Tigelaar, D. M.; Meador, M. A. B.; Bennett, W. R., Composite electrolytes for lithium batteries: Ionic liquids in APTES cross-linked polymers. *Macromolecules* **2007**, 40, (12), 4159-4164.
32. Rupp, B.; Schmuck, M.; Balducci, A.; Winter, M.; Kern, W., Polymer electrolyte for lithium batteries based on photochemically crosslinked poly(ethylene oxide) and ionic liquid. *European Polymer Journal* **2008**, 44, (9), 2986-2990.
33. Lu, Y. Y.; Moganty, S. S.; Schaefer, J. L.; Archer, L. A., Ionic liquid-nanoparticle hybrid electrolytes. *Journal of Materials Chemistry* **2012**, 22, (9), 4066-4072.
34. Schulze, M. W.; McIntosh, L. D.; Hillmyer, M. A.; Lodge, T. P., High-Modulus, High-Conductivity Nanostructured Polymer Electrolyte Membranes via Polymerization-Induced Phase Separation. *Nano Letters* **2014**, 14, (1), 122-126.
35. Grande, L.; von Zamory, J.; Koch, S. L.; Kalhoff, J.; Paillard, E.; Passerini, S., Homogeneous Lithium Electrodeposition with Pyrrolidinium-Based Ionic Liquid Electrolytes. *ACS Appl. Mater. Interfaces* **2015**, 7, (10), 5950-5958.
36. MacFarlane, D. R.; Sun, J.; Golding, J.; Meakin, P.; Forsyth, M., High conductivity molten salts based on the imide ion. *Electrochimica Acta* **2000**, 45, (8-9), 1271-1278.
37. Wong, S.; Vaia, R. A.; Giannelis, E. P.; Zax, D. B., Dynamics in a poly(ethylene oxide)-based nanocomposite polymer electrolyte probed by solid state NMR. *Solid State Ionics* **1996**, 86-8, 547-557.
38. MacFarlane, D. R.; Meakin, P.; Sun, J.; Amini, N.; Forsyth, M., Pyrrolidinium imides: A new family of molten salts and conductive plastic crystal phases. *Journal of Physical Chemistry B* **1999**, 103, (20), 4164-4170.
39. Wang, H. P.; Huang, H. T.; Wunder, S. L., Novel microporous poly(vinylidene fluoride) blend electrolytes for lithium-ion batteries. *Journal of the Electrochemical Society* **2000**, 147, (8), 2853-2861.
40. Feher, F. J.; Schwab, J. J.; Soulivong, D.; Ziller, J. W., Synthesis, characterization and reactivity of cis-cis-cis (C<sub>6</sub>H<sub>5</sub>)<sub>4</sub>Si<sub>4</sub>O<sub>4</sub>(OH)<sub>4</sub>. *Main Group Chemistry* **1997**, 2, (2), 123-132.
41. Henderson, W. A.; Passerini, S., Phase behavior of ionic liquid-LiX mixtures: Pyrrolidinium cations and TFSI- anions. *Chemistry of Materials* **2004**, 16, (15), 2881-2885.
42. Chinnam, P. R.; Mantravadi, R.; Jimenez, J. C.; Dikin, D. A.; Wunder, S. L., Lamellar, Micro-phase Separated Blends of Methyl Cellulose and Dendritic Polyethylene Glycol, POSS-PEG. *Carbohydrate Polymers* **2016**, CARP10290, pp. 19-29.

43. Cheng, H.; Zhu, C. B.; Huang, B.; Lu, M.; Yang, Y., Synthesis and electrochemical characterization of PEO-based polymer electrolytes with room temperature ionic liquids. *Electrochimica Acta* **2007**, *52*, (19), 5789-5794.
44. Vedarajan, R.; Ogawa, M.; Matsumi, N., Lithium ion conductive behavior of TiO<sub>2</sub> nanotube/ionic liquid matrices. *Nanoscale Research Letters* **2014**, *9*, 4.
45. Bruce, P. G.; Evans, J.; Vincent, C. A., Conductivity and transference number measurements on polymer electrolytes. *Solid State Ionics* **1988**, *28*, 918-922.
46. Evans, J.; Vincent, C. A.; Bruce, P. G., Electrochemical measurement of transference numbers in polymer electrolytes. *Polymer* **1987**, *28*, (13), 2324-8.
47. Medronho, B.; Lindman, B., Competing forces during cellulose dissolution: From solvents to mechanisms. *Curr. Opin. Colloid Interface Sci.* **2014**, *19*, (1), 32-40.
48. Lindman, B.; Karlstrom, G.; Stigsson, L., On the mechanism of dissolution of cellulose. *J. Mol. Liq.* **2010**, *156*, (1), 76-81.
49. Dawsey, T. R.; McCormick, C. L., The lithium chloride/dimethylacetamide solvent for cellulose- a literature review. *J. Macromol. Sci.-Rev. Macromol. Chem. Phys.* **1990**, *C30*, (3-4), 405-440.
50. Dupont, A. L., Cellulose in lithium chloride/N,N-dimethylacetamide, optimisation of a dissolution method using paper substrates and stability of the solutions. *Polymer* **2003**, *44*, (15), 4117-4126.
51. Ostlund, A.; Lundberg, D.; Nordstierna, L.; Holmberg, K.; Nyden, M., Dissolution and Gelation of Cellulose in TBAF/DMSO Solutions: The Roles of Fluoride Ions and Water. *Biomacromolecules* **2009**, *10*, (9), 2401-2407.
52. Brendler, E.; Fischer, S.; Leipner, H., Li-7 NMR as probe for solvent-cellulose interactions in cellulose dissolution. *Cellulose* **2001**, *8*, (4), 283-288.
53. Zhou, R.; Pramoda, K. P.; Liu, W.; Zhou, D.; Ding, G.; He, C.; Leong, Y. W.; Lu, X., Electrospun poly(vinylidene fluoride) copolymer/octahydroxy-polyhedral oligomeric silsesquioxane nanofibrous mats as ionic liquid host: enhanced salt dissociation and its function in electrochromic device. *Electrochimica Acta* **2014**, *146*, 224-230.
54. MacFarlane, D. R.; Meakin, P.; Amini, N.; Forsyth, M., Structural studies of ambient temperature plastic crystal ion conductors. *Journal of Physics-Condensed Matter* **2001**, *13*, (36), 8257-8267.
55. Joost, M.; Kunze, M.; Jeong, S.; Schoenhoff, M.; Winter, M.; Passerini, S., Ionic mobility in ternary polymer electrolytes for lithium-ion batteries. *Electrochimica Acta* **2012**, *86*, 330-338.
56. Gouverneur, M.; Jeremias, S.; Schoenhoff, M., Li-7 nuclear magnetic resonance studies of dynamics in a ternary gel polymer electrolyte based on polymeric ionic liquids. *Electrochimica Acta* **2015**, *175*, 35-41.
57. Ye, H.; Huang, J.; Xu, J. J.; Khalfan, A.; Greenbaum, S. G., Li ion conducting polymer gel electrolytes based on ionic liquid/PVDF-HFP blends. *Journal of the Electrochemical Society* **2007**, *154*, (11), A1048-A1057.
58. Moganty, S. S.; Jayaprakash, N.; Nugent, J. L.; Shen, J.; Archer, L. A., Ionic-Liquid-Tethered Nanoparticles: Hybrid Electrolytes. *Angewandte Chemie-International Edition* **2010**, *49*, (48), 9158-9161.